Critical assessment of solvent effects on absorption and fluorescence of 3HF in acetonitrile in the QM/PCM framework: A synergic computational and experimental study

Daniele Loco, Stefano Protti, Benedetta Mennucci, Alberto Mezzetti

Version of Record: https://www.sciencedirect.com/science/article/pii/S0022286018315187
Manuscript_7f56bd6487dcb37871af8248d09824bc

Critical assessment of solvent effects on absorption and fluorescence of 3HF in acetonitrile in the QM/PCM framework: a synergic computational and experimental study

Daniele Loco[1*], Stefano Protti[2], Benedetta Mennucci[3], Alberto Mezzetti[4*]

[1] *Laboratoire de Chimie Théorique, Sorbonne Université, CNRS, Paris, 75252, France.*

[2] *PhotoGreen Lab, Department of Organic Chemistry, University of Pavia, Via Taramelli 12, 27100 Pavia, Italy*

[3] *Department of Chemistry, University of Pisa, via G. Moruzzi 13, 56124 Pisa, Italy*

[4] *Laboratoire de Réactivité de Surface, UMR CNRS 7197, Sorbonne Université, 4 Pl. Jussieu, 75005 Paris, France*

**corresponding authors*

Abstract

Absorption and fluorescence properties of 3-hydroxyflavone (3HF) dissolved in the polar aprotic solvent acetonitrile have been investigated by electronic spectroscopies, associated to mixed quantum mechanical/classical calculations, where the effect of the solvent is included at the classical level by means of the polarizable continuum model (QM/PCM).

Whereas absorption and fluorescence (λ_{exc} = 342 nm) spectra confirmed previous results, a detailed spectrofluorimetric investigation of the anion, deriving from solvent-induced deprotonation of the OH group of 3-hydroxyflavone, showed for the first time that a single anionic form is present in solution, differently from what observed in another polar aprotic solvent, DMSO.

A detailed computational study using five different functionals has been carried out in order to reproduce and better understand absorption and emission bands on the different existing forms for 3HF in solution: Normal (N), Tautomer (T), Anion (A).

The results are discussed in terms of solvent effects on 3HF spectroscopic properties. It was found that simulations are in good agreement with the spectroscopic data for the N and T forms, whereas for the A form larger discrepancies are observed, especially for absorption properties. The effect of specific solute solvent hydrogen bond interactions involving the C=O and OH moieties of 3HF was also explored, aiming to better simulate anionic spectroscopic properties. Results suggest that a more complete description of the whole solvation shell is necessary.

1. Introduction

In several research fields there is a strong interest in environment-sensitive fluorophores [1]. Naturally-occurring flavonols [2] and 3-hydroxychromones [3] are widely used. For nearly 40 years, 3-hydroxyflavone, also called 3HF (the simplest among the flavonols, and possibly the most used among the synthetic molecules possessing the 3-hydroxychromone core) has been extensively used as a fluorescent probe, and its sensitiveness to the environment studied by a variety of approaches [4].

Upon excitation, 3HF normally undergoes a Excited-State Intramolecular Proton Transfer (ESIPT), with the proton moving from the 3-OH group to the carbonyl, to give the $C=OH^+$ moiety. The intramolecular hydrogen bond between 3-OH and the C=O plays a key role for ESIPT, as it represents the path for this transfer to occur. However, ESIPT is often hampered by 3HF interactions with its environment, which can partially break the intramolecular hydrogen bond. Indeed, in most cases two competitive pathways are observable from the photoexcited state ^{1}N*, namely emitting decay to N and ESIPT to the excited tautomer ^{1}T* (scheme 1). As a consequence, excitation of 3HF may result in a dual fluorescence at ca. 400 nm (hν from ^{1}N*, scheme 1) and 510-540 nm (hν' from ^{1}T*, scheme 1), respectively [5]. In the latter case, the obtained ground state tautomer (T) undergoes to a thermal back proton transfer (*path **b***) to give the resting N state. ESIPT alone occurs in inert media such as apolar solvents [6], superfluid helium nanodroplets [7] and Shpol'skii matrices [8] (structure a in Fig. 1); only emission from ^{1}T* is observed.

In polar or H-bonding media the situation is different. Two types of interactions of 3HF with the surrounding environment are observed: 1) specific hydrogen-bonding interactions involving the C=O and 3-OH moieties of 3HF [9] and 2) long range solvent polarization interactions [10]. Therefore, the photophysical properties of 3HF are extremely sensitive to the physicochemical properties of its surrounding molecular microenvironment.

Actually, 3HF photophysics has become a model system not only to rationalize the behaviour of similar environment-sensitive fluorescent probes, but also to investigate ESIPT [11]: specific solute/solvent interactions, as well as the efficiency of ESIPT, can be studied through easy observable spectroscopic parameters, such as the absorption spectrum, the relative intensity of the emission ^{1}N* and ^{1}T* bands, the wavelength of the two emission peaks, or the lifetime of the ^{1}N* and ^{1}T* emissions.

The scenario is further complicated by the possibility of environment-induced deprotonation of the 3-OH group, leading to 3HF anion whose photophysical properties are completely different

from those of neutral 3HF [12]. Absorption of 3HF anion is in the 400-500 nm range, according to the environment, whereas emission is normally in the 460-500 nm range, but in some cases it can extend to 530 nm [13]. Absorption and emission bands depend strongly on the interaction of the anion with its environment, as well as on the characteristics of its counter ion [13].

These aspects have been investigated in details for DMSO solutions [13, 14], where theoretical calculations to simulate absorption and emission spectra have suggested the presence of both an H-bonded anion−protonated solvent ion pair and of the bare 3HF anion.

The peculiar emission properties of 3HF have been exploited in a wide range of applications, such as lasers [15], wavelength shifter devices [16], in scintillators [17], sharp-cut optical filters [18] and other photonic devices [19].

The main photochemical applications of 3HF are, however, related to its environment-sensitive emission properties, in bioanalytical [20], physical [21] and biophysical chemistry [22]. It should be added that in the last 20 years several 3HF derivatives with specific, tailored properties have been developed and used for many purposes [4], mainly in biology [3].

Despite the experimental efforts and the theoretical analyses presented so far (see [6, 9-14, 23-25] and refs therein), a complete rationalisation of such solvent effects on 3HF spectroscopic properties is still lacking.

The last decades have seen major advances in computer sciences as well as in the computational power offered by technological improvements. Thanks to such technical evolutions, more reliable computational models have been devised and applied to real-life chemical problems, including the field of solvation, or more generally environment effects on solute properties.

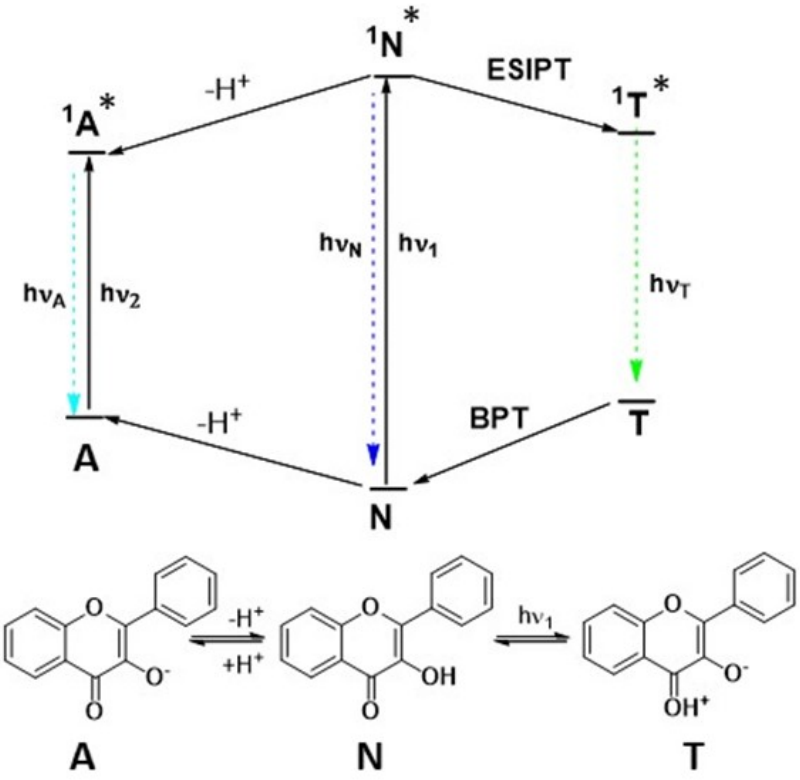

Fig. 1. Energy level scheme for the Normal (N), Tautomeric (T), and anionic forms (A) of 3HF

Since many years the QM/classical approaches [26-33] have been extended to treat excited state properties, especially in the Time Dependent Density Functional Theory (TDDFT) framework, mainly due to its good accuracy/efficiency ratio. A peculiar feature appears in this context when a polarizable embedding is applied (either as continuum or atomistic). Within a polarizable embedding a new contribution arises due to the dynamic response of the polarizable environment. Such contribution is calculated through the transition densities corresponding to the different excitations.

In this paper we report the investigation, by a synergic strategy associating electronic spectroscopies (UV-Vis and fluorescence) and a QM/Classical approach, based on TDDFT and a continuum description of the solvent, on 3HF in acetonitrile (ACN).

Indeed, several research papers involving experimental data on 3HF in ACN have been reported in the literature.

The reactivity of 3HF towards singlet [34] as well as the DPPH-initiated 3HF oxygenation [35] have been studied in this solvent. ACN has also been used to investigate the complexation of alkaline metals perchlorates by 3HF [36-37]. 3HF vibrational spectra in ACN have been reported and simulated [38-39]. However, the most relevant fields have been the study of 3HF photochemistry [40**]** and 3HF photophysics [10; 12; 39; 41-42]. The ACN-induced

deprotonation of 3HF has also been investigated, and the photophysical properties of the formed anion studied [12; 43].

To our knowledge, theoretical studies on 3HF in acetonitrile so far have concerned structural DFT calculations [39], ESIPT dynamics [23] and 3HF reactivity towards singlet oxygen [44].

2. Experimental section

2.1. Chemicals and Spectroscopy

3-Hydroxyflavone (3HF) was purchased from Sigma-Aldrich and recrystallized twice from cyclohexane before use. ACN (Carlo Erba, HPLC grade) has been dried by distillation over CaH_2 before use. UV-Vis absorption spectra were recorded on a Jasco V-550 Spectrophotometer. Emission spectra were recorded by means of a LS-55 spectrofluorometer (Perkin Elmer). Quartz cuvettes (optical path: 10 mm) were used, except in the case of solution at higher concentrations (4.2×10^{-4}, 2.5×10^{-3} and 10^{-2} M) where quartz cuvettes with an optical path of 1.0 and 0.1 mm, have been employed.

2.2 QM calculations

The molecular geometries of all 3HF forms, namely the normal (N), tautomeric (T) and anionic (A), are obtained from geometry optimizations in presence of acetonitrile solvent (ACN, ε = 35.688), modeled by means of the polarizable continuum model (PCM) [32] in its integral equation formalism (IEF) version [45-46]. Also the lowest electronic excited state (ES) geometries of the different forms were optimized, in order to simulate the fluorescence emission spectra.

Following the computational protocol proposed in [14], ground state (GS) optimizations were performed with the hybrid B3LYP exchange-correlation functional, with a 6–31G(d,p) Pople basis set. As explained in the “Results and discussion” section, in some cases GS optimization were performed with other functionals, in order to assess any possible influence of the choice of the functional on the optimized geometry. ES optimizations were performed at time-dependent (TD)B3LYP/6–31G(d,p) within an equilibrium approach for the continuum solvent. In addition, in some specific cases (see “Results and discussion” section) an approach where also one or two solvent molecules are included at QM level - while the rest of the solvent is

still modeled with the PCM model - was used. In the rest of this work we will refer to the first approach, where the solvent is completely described at the PCM level, with the QM/PCM acronymous. The second approach (with some solvent molecules included at the QM level) will be referred to as QM(ME)/PCM.

Excitation and emission processes were simulated using a TDDFT approach. The performances of a series of hybrid functionals were tested. These functionals were: B3LYP[47], PBE0 [48] and M062X [49], and two long-range corrected (LC) functionals, namely the CAM-B3LYP [50] and ωB97X [51], The CAM-B3LYP performances were already tested against those of B3LYP for the 3HF forms in DMSO [14]; the second one was found to give better results. The B3LYP functional has also been used in a previous work by another research group [39].

The effect of the basis set has also been tested; double- and triple-ζ Pople basis set, enriched at different levels with polarization and diffuse functions, plus an augmented correlation-consistent (aug-cc) triple-ζ Dunning basis were used. All calculations were performed with Gaussian16 [52].

2.3 Excited state solvation models

When the TDDFT formalism is applied in the context of classical polarizable embeddings, the (in principle) complete spectrum of the excitations is determined simultaneously by solving for the poles of the proper response function. Such response function includes the explicit response due to the polarizable environment. This formulation is also known as “Linear Response” (LR) model.

The LR-TDDFT model has been shown to properly describe the dynamic environment effect in excitations involving bright states, characterized by a large transition dipole moment [53].

The lack of capability of such approach in describing the relaxation of the environment in response to the changes in the QM density related to the excitation process is also well-known. It is reflected in the difficulties of such model in reproducing and describing excitations involving large changes in the electron density, as in the Charge–Transfer (CT) like excitations. To overcome such kind of problems, a state–specific (SS) description related to the environment response is required [54-58].

The simplest and most effective formulation, usually called “corrected Linear Response” (c–LR) scheme [54] , uses a relaxed density matrix for the specific excited state of interest. In the case of continuum model, (present work), after the selection of the excited state of interest, the corresponding excitation energy is corrected for the interaction with the proper induced surface charges. Due to the different physical origin, and interpretation, of the LR and SS response components, their combination has been proposed to achieve a more complete and correct description of embedding effects on electronic excitations. [59-61].

For this reason a combination of the LR and c-LR was used to simulate the excitation properties of 3HF (N, T, A forms) in ACN.

3. Results and discussion

3.1. UV-Vis and fluorescence spectroscopy

The UV-Vis spectrum and the fluorescence spectrum upon excitation at 342 nm of 3HF in ACN are shown in Fig. 2. They are consistent with previous reports [12, 40]; the UV-Vis spectrum shows two absorption bands at 305 and 342 nm. The emission spectrum shows the characteristic dual fluorescence observed for 3HF in polar and protic media, with peaks at 395 and 525 nm, characteristic of the ^{1}N* and of the ^{1}T* form, respectively.

The UV-Vis spectrum shows also an extremely weak shoulder extending beyond 400 nm. Bands in this spectral region have previously been attributed to 3HF anionic form(s) [12, 43].

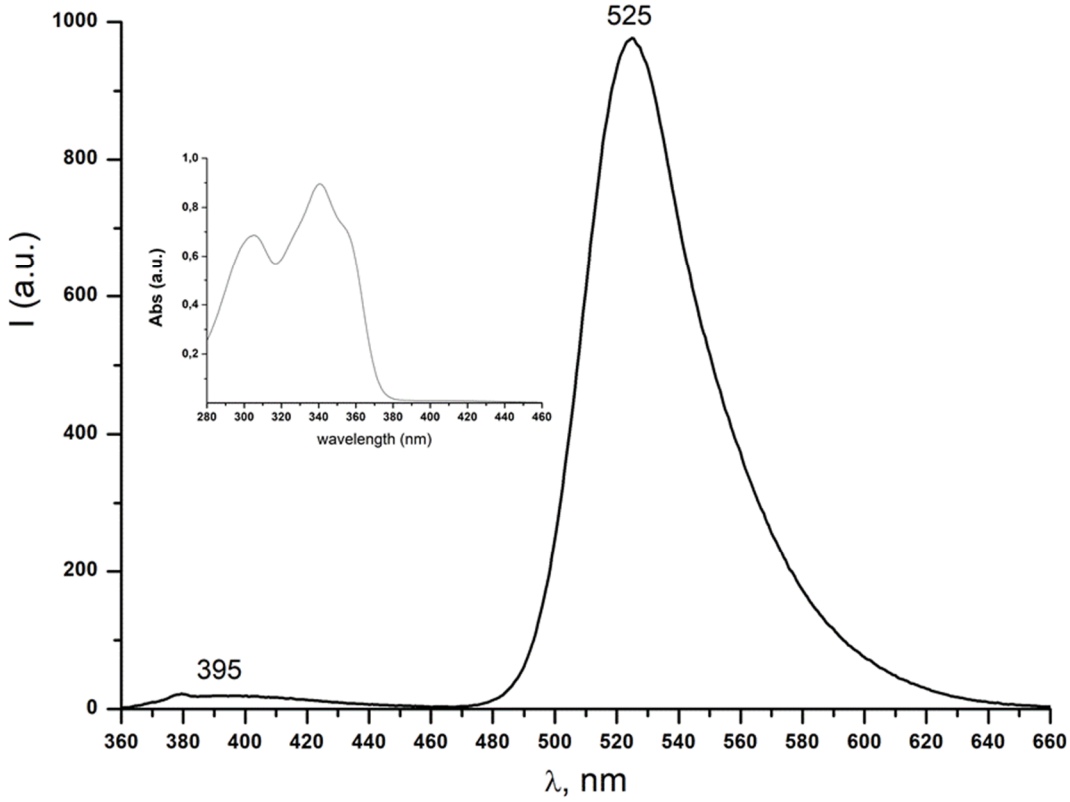

Fig. 2. Fluorescence spectrum (λ_{exc}= 342 nm) and absorption spectrum (inset) of 3HF in ACN (4.2×10^{-5} M).

Fig. 3 shows the fluorescence spectrum upon excitation at different wavelengths in the 405-430 nm region. The emission spectra are essentially equivalent, with a fluorescence maximum observed at 467 nm. Only slight variations in the fluorescence peak intensity are observed upon changing the excitation wavelength between 405 and 430 nm. This strongly suggests that only one 3HF anionic species is present in ACN. This result is at odds with the presence of two different 3HF anionic species observed in DMSO (interpreted as a 3HF anion hydrogen bonded to $DMSOH^+$, the protonated DMSO molecule that abstracted the H^+ to produce the anion, and the "free" 3HF anion) [13]. These two anionic species observed in DMSO were characterized by different absorption and emission properties, with the $3HF^- \cdots DMSOH^+$ species absorbing at 428 nm and emitting at 502 nm, and the "free" $3HF^-$ absorbing at 485 nm and emitting at 529 nm [13].

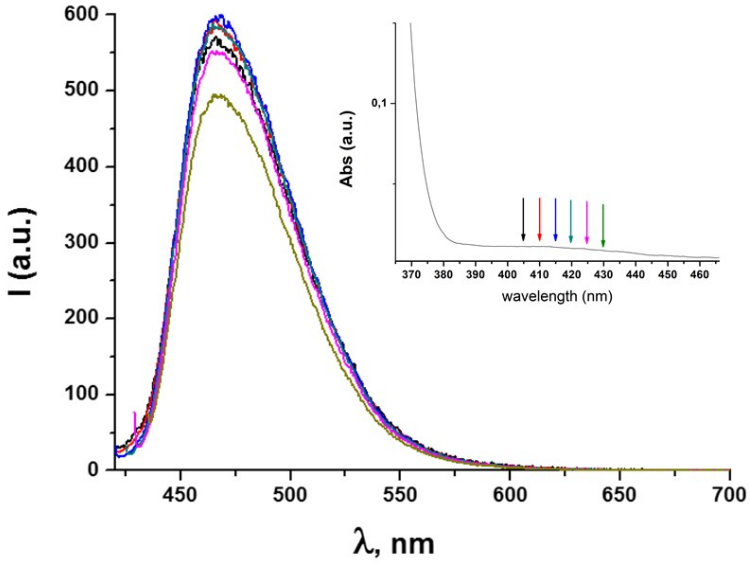

Fig. 3. Fluorescence spectra of 3HF solutions in ACN (2,5 x 10^{-3} M) exciting in spectral region where the anionic form of 3HF absorbs. Inset: absorption spectrum of 3HF in ACN. The different excitation wavelength for the fluorescence spectra are indicated by arrows.

In order to exclude the presence, in very small amounts, of a second anionic species absorbing at higher wavelength, fluorescence spectra were recorded also upon excitation at $\lambda_{exc} > 450$ nm in 3HF solution in ACN at different concentration, in the 10^{-5}-10^{-2} mol L^{-1} range. No emission was observed, even at high concentration[1].

Fluorescence excitation spectra were also recorded at four different emission wavelengths between 465 and 480 nm, i.e. the region where 3HF anion fluorescence was observed and where neutral 3HF dual fluorescence should not contribute significantly. As shown in Fig. 4, excitation spectra are comparable, thus the presence of more than one anionic emitting species can therefore be excluded. The shoulder observed at ~380 nm in the excitation spectrum (Figure 4) recorded at λ_{em} = 480 nm was assigned to the residual emission from the T-form of neutral 3HF. (Note that it was not possible to observe any signal at wavelength below 370 nm due to the high absorbance of 3HF in that region).

It is important to underline that the position of the absorption band (and of the fluorescence excitation band) does not provide any information on the nature of the anionic form, especially

[1] Parallel UV-Vis spectra at the same concentrations showed that no shift in band position for 3HF absorption, excluding thereby formation of dimers or aggregates.

on the presence or absence of the absence of a hydrogen bond involving the oxygen of the anion. In fact, it has already been shown that position of the absorption band of the anion can vary significantly, even when comparing relatively “similar” situations [13]. Only a computational investigation can provide information on the structure of the anion, and on its interactions with the solvent (see Section 3.2).

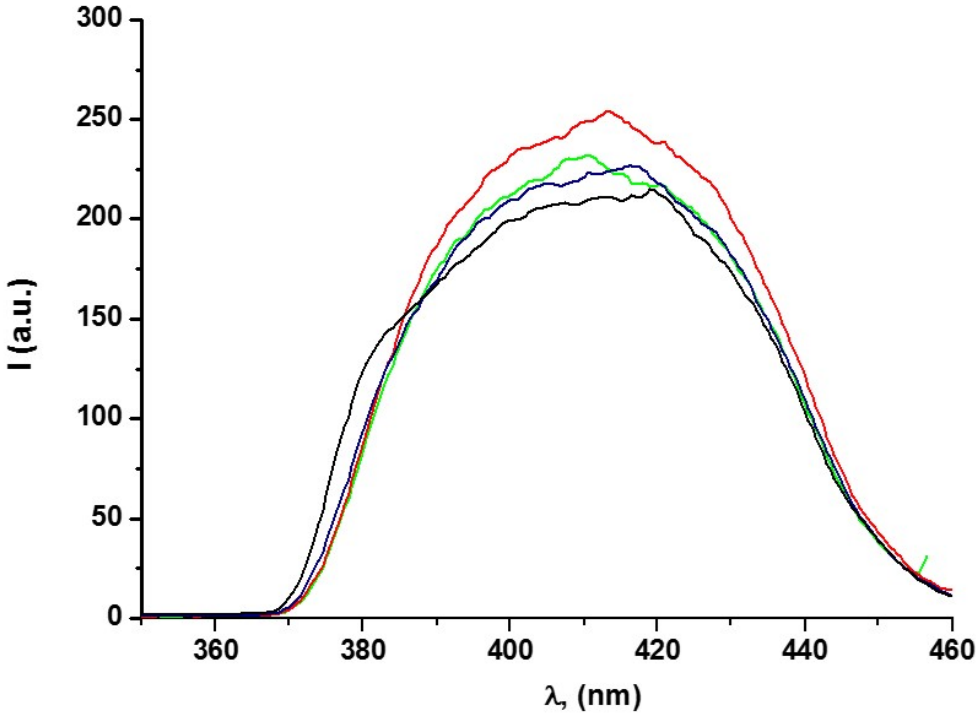

Fig. 4. Fluorescence excitation spectra of 3HF solutions (2,5 x 10^{-4} M) recorded at different emission wavelengths: λ_{em} at 465 nm (red line), 470 nm (green line), 475 nm (blue line) and 480 nm (black line).

3.2 Functional benchmarking on the absorption properties

A preliminary assessment of the DFT exchange-correlation functional suitable for the problem under investigation was performed. For this purpose the computed excitation energies were compared to the experimental absorption maxima measured for the N and A forms of 3HF (the absorption spectrum of the T form cannot be measured directly). The final goal is to select a good functional for all forms of 3HF.

In our benchmark hybrid functionals are mainly compared with hybrid LC ones. LC functionals have been developed to improve the description of long-range electron-electron exchange interaction [62] and therefore they should be better suited for extended systems with delocalized electrons. They are also expected to improve the description of charge transfer (CT) states [63-66]. It should be taken into account that hybrid functionals partially mitigate pure DFT

functionals failure in describing CT, introducing some percentage of Hartree-Fock (HF) exact exchange [63, 67-68].

As stated in our previous work on 3HF in DMSO and chloroform [14], all the electronic transitions responsible of the absorption of the N, T and A forms of 3HF have a clear $\pi\pi^*$ character, with some (CT) character for the second transition of the N form.
Table 1 shows the comparison between the experimental values and the computed ones, within a QM/PCM approach, which has already shown to be successful for 3HF in DMSO and chloroform, for all the functionals selected: i) B3LYP, ii) PBE0, iii) CAM-B3LYP, iv) ωB97X and v) M062X. Also a signed error, computed as the energy difference between the calculated ($E_{calc.}$) and the experimental ($E_{exp.}$) value is reported.

Table 1.

Comparison between experimental maxima of measured linear absorption bands and computed excitations with the different functionals selected at the 6-31+G(d,p)/PCM level. The excitation values are followed by their differences, computed as $E_{calc.} - E_{exp.}$. Values are in eV or in nm (in parenthesis) computed on the optimized geometries at B3LYP/6-31G(d,p)/PCM level of theory. The only exception is represented by the Opt-ωB97X values, where TdωB97X calculations have been performed on structures optimized at ωB97X/6-31G(d,p)/PCM level.

	B3LYP	PBE0	CAM-B3LYP	ωB97X	M062X	Opt-ωB97X	Experiment
N	3.47 (357)	3.57 (347)	3.83 (324)	3.99 (311)	3.88 (320)	4.14 (299)	3.63 (342)
	4.05 (306)	4.17 (297)	4.47 (277)	4.61 (269)	4.52 (274)	4.75 (261)	4.07 (305)
A	2.57 (482)	2.65 (468)	2.91 (426)	3.08 (403)	2.93 (423)		2.95 (420)
	$E_{calc.} - E_{exp.}$						
N	-0.16	-0.06	0.20	0.36	0.25	0.51	
	-0.2	0.11	0.41	0.54	0.46	0.68	
A	-0.38	-0.30	-0.04	0.13	-0.02		

This comparison shows that the choice of the functional is not straightforward. When the N form is considered, it is clear that the B3LYP and the PBE0 perform better than the other functionals, which underestimate the excitation value of the lowest transition of 0.16 and 0.06 eV, respectively. For the first transition of the N absorption spectrum the PBE0 value shows the best agreement with the experimental value. While the B3LYP error for the first transition is comparable, in absolute value, to those of CAM-B3LYP and M062X, this functional results the best for the second transition, with the lowest signed error. Beside the PBE0, all other functionals show an error larger than 0.4 eV for the second transition.

Concerning structure optimization, as mentioned previously, the N structure was optimized with the B3LYP functional in all cases but one, where the LC functional ωB97X was used, to assess any possible effect of the functional on the geometry.

The excitation energy was calculated with the same functional. The predicted values are even worse than those computed on the B3LYP structure (see Opt-ωB97X in Table 1).

The scenario seems to be reversed when we compute the first transition of the absorption spectrum of the A form of 3HF. Good or fairly good signed errors are obtained for the CAM-B3LYP, ωB97X and M062X functionals, whereas unsatisfactory results (all lower than the reference) are obtained for B3LYP and PBE0. The latter shows an absolute error close to that of the ωB97X, while the B3LYP gives the worst agreement with the experiment (-0.38 eV). For this excitation CAM-B3LYP and M062X have the best performances with a positive signed error in the order of 10^{-2} eV.

Such differences in the performance of the functionals can be partially related to some error compensation due to the particular functional form adopted.

Another possible source of error is the basis set convergence. The excitation values for the N, T, and A forms of 3HF were computed with four additional basis, namely the 6-311+G(d,p), 6-311++G(d,p), 6-311++G(3df,3pd) and aug-cc-pvtz, each with B3LYP, PBE0 and the ωB97X functionals, with the latter chosen as representative for the LC family. The absorption properties were found to be almost completely insensitive to any increase of the basis set. As a consequence, the 6-31+G(d,p) was used for any following calculation. The corresponding results are reported in the Supplementary Data.

These results show how ambiguous is, in this case, to rely on a simple comparison between computed and measured excitation energies in order to choose the best functional for all the transitions of interest. A deeper investigation on the nature of the excitations involved and on how the used functionals can behave in treating them is needed. To this aim we have analyzed the electronic transition densities by means of the natural transition orbitals (NTOs) [69] for the N, T and A species (Fig. 5).

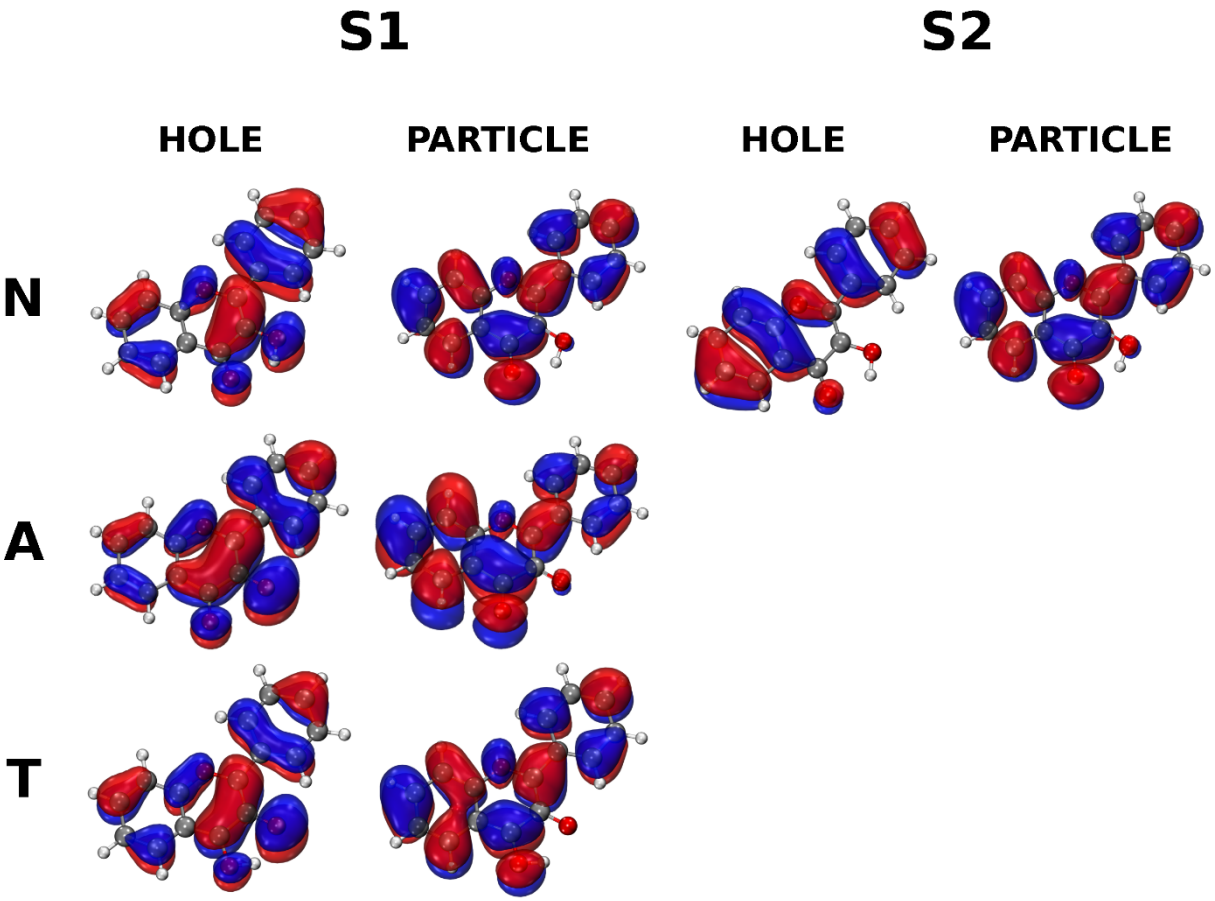

Fig. 5. N, T and A form NTOs computed at PBE0/6-31+G(d,p) level are reported. S1 is used as label to identify the lowest N transition and the only T and A excitation which is detected experimentally, while S2 is used for the second transition of the N form

The NTOs confirm the $\pi\pi^*$ nature, especially for the first transition of the N and of the A forms. The NTOs have been computed with the PBE0/6-31G+(d,p)/PCM method. No significant difference was observed in the NTOs computed with the CAM-B3LYP functional (see Supplementary Data). Very interestingly, the shape of these NTOs clearly show that the character of the first transition is very similar in both the N and the A form of 3HF. Therefore, the first transition in the N and A form should be described by the two families of functionals (hybrids and LC) in a comparable way.

Conversely, the benchmark (see Table 1) shows that the LC functional and the M06-2X seem particularly well-suited to describe the absorption spectrum of the A form, but they are much less accurate for both the transitions concerning the N state. B3LYP and PBE0 behave, as expected, in a similar way, with very good results for the N form and larger errors (around 0.3 eV) for the A absorption.

In view of these observations, no motivations are found to choose different functionals for different transitions. The PBE0 functional was chosen instead, since it shows in average the best performance when both the N and the A form are considered. It is worth mentioning that a more careful analysis of the excited state properties may reveal more refined differences between the excitations in the N and A form and which are hidden in the simple NTO inspection. More specific techniques based, for example, on the one-particle transition density matrix [70-73] and indexes specially made for the characterization of excited state transitions can strongly enforce, or contradict, the arguments we used in the selection of the functional. Furthermore, the representation of the anionic form may suffer of problems in its DFT description also in the ground state, which would be reflected also in the excitation properties. Such analysis, however, is beyond the scope of this work.

From the data reported in Table 1 we can conclude that the PBE0/PCM results for the two lowest excitations of the N form are in good agreement with the experimentally observed absorption maxima. For the T form, whose experimental absorption is not available, the excitation energy is calculated to be very close to that of the anionic form. As far as the A form is concerned, the experimental absorption band is found around 420 nm (2.95 eV, see experimental part), quite far from the computed value of 468 nm (2.65 eV). This computed value is much more in agreement with the measured value and the computed value for the free anion in DMSO [14] as well as in basic conditions or in other solvents [13].

Beside any previous observation about the choice of the functional, another possibility to explain the larger discrepancies observed with respect to the experimental data is the presence of specific solute-solvent interactions. In the case of DMSO, for instance, it has been proposed that a hydrogen bond is formed between the OH group of 3HF and a DMSO molecule to form a solute-solvent "complex"; similarly, it has been proposed that a hydrogen bond is formed between the anionic form of 3HF and a protonated DMSO molecule ($DMSOH^+$), to form another solute-solvent "complex" [13]. The existence of these complexes has been suggested also by TD-DFT calculations from our groups [14]. The possible formation of similar complexes has been also considered in the case of 3HF in ACN [12].

In the present work, the effect of specific solute-solvent interactions was simulated by applying the QM(ME)/PCM scheme to calculate the N and A form absorption spectra. One ACN solvent molecule was introduced in the QM region in two different configurations, as reported in Fig. 6. In the first configuration, the ACN nitrogen is directly oriented towards the hydrogen of the OH group of 3HF. In the second configuration the ACN molecules is interacting with 3HF also through a H_2C-H···O=C hydrogen bond (Configuration 2). The rationale of this choice is that

according to solvent and solute hydrogen bonding scales, ACN is characterized by a relatively high hydrogen bond accepting basicity and by a quite low, but non-zero, hydrogen bond donating acidity ([12] and refs. therein). These structures have been optimized at the same level of theory reported in Subsection 2.1.

The effect of these specific interactions seems to be completely negligible (in the order of 0.01 eV), as the computed absorption values are completely unaffected, remaining the same as that computed in the QM/PCM scheme. We reported these values in table 2.

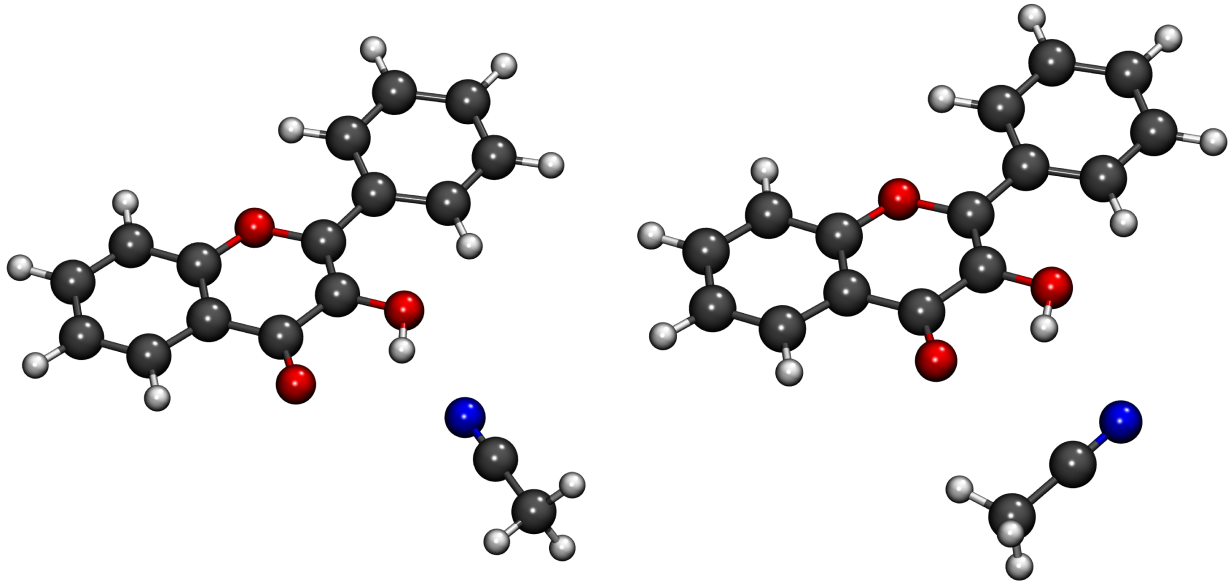

Fig. 6. The two possible configurations of 3HF interacting through hydrogen bond(s) with one explicit ACN molecule, therefore included in the quantum portion of the system for the QM(ME)/PCM approach. Left panel: configuration 1, only one hydrogen bond, between the 3-OH group of 3HF and the nitrogen atom of ACN. Right panel: configuration 2, where two hydrogen bonds are present: 3-OH···N, as in the left panel, and H_2C-H···O=C (the methyl group of ACN acting as a donor and the carbonyl of 3HF as acceptor). See text for further details.

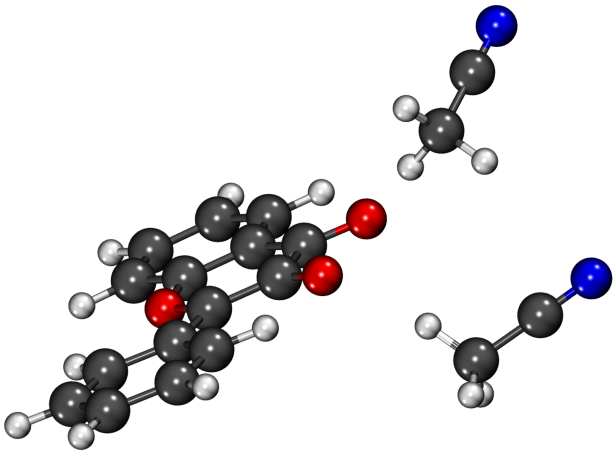

Fig. 7. 3HF anion interacting (as an acceptor) through hydrogen bonds with two ACN molecules (their methyl group being the hydrogen bond donor). See text for further details.

Table 2.

Excitation energies computed for the two 3HF N configurations where a single ACN molecule is included in the QM portion, as reported in Fig. 6 (See text and caption of Fig. 6 for the definition of Configuration 1 and 2) and for the only configuration of the A form with two explicit ACN molecules included in the QM portion (see Fig. 7). All values are computed at the PBE0/6-31+G(d,p)/PCM level, and are reported in eV.

	N	A
Configuration 1	3.55	2.71
	4.23	-
Configuration 2	3.56	-
	4.19	-

The same QM(ME)/PCM approach was applied to the A form of 3HF. Two ACN molecules were included in the QM part, with the methyl hydrogens pointing towards the oxygen atoms of 3HF anions where the highest charge density should lie, as the chemical intuition suggests (see Figure 7). Two hydrogen bonds are therefore formed. As in the N form case, the inclusion of few explicit solvent molecules in the QM region has no significant effect on the absorption properties, and in this case does not recover the gap between the experiment and the simulation, even though the excitation energy changes in the right direction, increasing to 2.71 eV. This result can suggest that a larger network of solvent interactions with 3HF could be the origin of the experimentally observed, blue-shifted absorption of the A form.

As in the case of DMSO [14] the hypothesis of the existence of a complex formed by one molecule of protonated solvent and the anionic form of the 3HF was made, the $ACNH^+$ molecule being the result of a ground state intermolecular proton transfer from the N form of 3HF to the nitrogen of one ACN solvent molecule. Such solute-solvent complex could be predominant in solution (as hypotized for DMSO) and therefore responsible for the absorption band observed experimentally for the A form. As already observed in the case of DMSO [14], such complex does not correspond to an energy minimum, when trying an optimization at PBE0(ME)/PCM level. Without any constrain in the optimization procedure, the proton artificially placed on the ACN molecule rapidly relaxes back on the 3HF oxygen. The same result is also obtained if two additional ACN molecules are added (interacting through hydrogen bonds with the two oxygens of the anion), see Supplementary Data.

More extended solute-solvent interactions involving more ACN solvent molecules around 3HF may favour the ground state proton transfer, but such analysis is beyond the scope of the present work.

3.3 Emission simulation

The same procedure applied for the absorption has been carried out for the emission properties of 3HF in ACN, relying on the same level of theory assessed for the absorption. In ACN, along with $^1T^*$ fluorescence, $^1N^*$ fluorescence can also be observed, as the formation of hydrogen bonds between ACN and 3HF hampers ESIPT. We recall that ACN molecules can act both as acceptors and donors of hydrogen bonds. In Table 3 the experimental fluorescence energies are compared to those computed within the different solvation schemes.

Table 3

Comparison between calculated and experimental emissions for the 3HF forms. All the reported value are in eV, while the values in parentheses are in nm. All computed values refer to the PBE0/6-31+G(d,p) level of theory.

	Calculation	Experiment
N	3.16 (392)	3.07 (404)
N (Configuration 1)	3.17 (391)	
T	2.34 (530)	2.36 (525)
A	2.44 (508)	2.65 (468)
A (Configuration 1)	2.37 (523)	

Very good agreement is found for the N form and the T form (difference < 0.1 eV), whereas for the A form a larger error, as for the absorption, is observed, (0.21 eV). When the QM(ME)/PCM results are considered, the picture remains unchanged. For the N emission, we selected only one of the two solute-solvent configuration optimized (Configuration 1, see fig. 6), since the two configurations are equivalent, as shown by their equivalent absorption values. For the anion the agreement with the experiment is slightly worse compared to the QM/PCM value (which is already not satisfactory). As for the absorption, we can speculate that a more refined inclusion of solvent effects, adding more “explicit” solvent molecules (i.e. in the QM part), may recover at least part of the gap between the experiment and the calculations for the A form.

Finally, the effect of the functional on the geometry was tested also for the emission. The N and A excited states were optimized at the (TD)PBE0/6–31G(d,p) level. Whereas the emission computed for the N form remains almost the same, the emission of the A form becomes worse, very close to the one reported in table 3. The results are reported in Supplementary Information.

4. Conclusions

In this work, the absorption and emission properties of the different forms of 3HF in ACN (N, T, A) were studied, combining experimental and computational methods. Differently from the

situation found in another polar aprotic solvent (DMSO) only one anionic form – deriving from partial solvent-induced deprotonation of the 3-OH group of 3HF - has been detected.

We have selected an appropriate DFT exchange-correlation functional to compute the absorption and emission properties of the N, T, and A forms of the 3HF molecule, analyzing the NTOs related to the transition of interest, and comparing the excitation energies with the experimental values.

Our calculations match the experimental data in a satisfactory way for the absorption of the N form, and for the emission of both the T and N forms. On the other hand, the agreement is less satisfactory for the A form. This can be attributed to some specific solute-solvent interactions not considered in our QM/PCM and QM/ME/PCM models.

Further studies are needed in this direction. A possible computational approach to investigate more in details effects induced by the structure of the solvent around 3HF is a QM/MM approach.

References

[1] A.S. Klymchenko, Solvatochromic and Fluorogenic Dyes as Environment-Sensitive Probes: Design and Biological Applications, Acc. Chem. Res. 50(2) (2017) 366-375.

[2] P.K. Sengupta, Pharmacologically Active Plant Flavonols as Proton Transfer Based Multiparametric Fluorescence Probes Targeting Biomolecules: Perspectives and Prospects, Reviews in Fluorescence (2016) 45-70.

[3] A.S. Klymchenko, Y. Mely, Fluorescent environment-sensitive dyes as reporters of biomolecular interactions, Prog. Mol. Biol. Transl. Sci. 113 (2013) 35-58.

[4] S. Protti, A. Mezzetti, Any colour you like. Excited state and ground state proton transfer in flavonols and applications, Photochemistry 40 (2012) 295-322.

[5] P.K. Sengupta, and M. Kasha, Excited state proton-transfer spectroscopy of 3-hydroxyflavone and quercetin, Chem. Phys. Lett. 68(2-3) (1979) 382-385.

[6] D. Mc Morrow, M. Kasha, Intramolecular excited-state proton transfer in 3-hydroxyflavone. Hydrogen-bonding solvent perturbations. J. Phys. Chem. 88 (11) (1984) 2235-2243.

[7] R. Lehniga, D. Pentlehner, A. Vdovin, B. Dick, A. Slenczk, Photochemistry of 3-hydroxyflavone inside superfluid helium nanodroplets, J. Chem. Phys. 131 (2009) 194307.

[8] A. N. Bader, F. Ariese, C. Gooijer, Proton Transfer in 3-Hydroxyflavone Studied by High-Resolution 10 K Laser-Excited Shpol'skii Spectroscopy, J. Phys. Chem. A 106 (2002) 2844-2849.

[9] A. J. G. Strandjord, P. F. Barbara, The proton-transfer kinetics of 3-hydroxyflavone: solvent effects, J. Phys. Chem. 89 (11) (1985) 2355-2361.

[10] G. A. Brucker, D. F. Kelley, T. C. Swinney, Proton-transfer and solvent polarization dynamics in 3-hydroxyflavone, J. Phys. Chem. 95(8) (1991) 3190-3195.

[11] See for a recent review: V. I. Tomin in Hydrogen Bonding and Transfer in the Excited state, ed K-L. Han and G.-J. Zhao, John Wiley & Sons Ltd, Chichester, UK, 2010, vol I & II, pp. 463-523

[12] S. Lazzaroni, D. Dondi, A. Mezzetti, S. Protti, Role of solute-solvent hydrogen bonds on the ground state and the excited state proton transfer in 3-hydroxyflavone. A systematic spectrophotometric study. Photochem. Photobiol. Sci., 17 (2018) 923–933.

[13] S. Protti, A. Mezzetti, J.-P. Cornard, C. Lapouge, M. Fagnoni, Hydrogen bonding properties of DMSO in ground-state formation and optical spectra of 3-hydroxyflavone anion. Chem. Phys. Lett. 467 (2008) 88–93.

[14] D. Loco, N. Gelfand, S. Jurinovich, S. Protti, A. Mezzetti, B. Mennucci, Polarizable QM/Classical Approaches for the Modeling of Solvation Effects on UV−Vis and Fluorescence Spectra: An Integrated Strategy, J. Phys. Chem. A 122 (1) (2018) 390−397.

[15] P. Chou, D. McMorrow, T. J. Aartsma, M. Kasha, The proton-transfer laser. Gain spectrum and amplification of spontaneous emission of 3-hydroxyflavone, J. Phys. Chem. 88(20), (1984) 4596-4599.

[16] S. Protti, K. Raulin, O. Cristini, C. Kinowski, S. Turrell, A. Mezzetti, Wavelength shifting systems based on flavonols and their metal complexes encapsulated by post-doping in porous SiO_2 xerogel matrices, J. Mol. Struct. 993(1-3) (2011) 485-490 and references therein.

[17] E. Biagtan, E. Goldberg, R. Stephens, E. Valeroso, J. Harmon, Gamma radiation dose rate effects on a polymer scintillator containing a large Stokes shift dye, 3-hydroxyflavone. Nucl. Instrum. Methods Phys. Res., Sect. B, 114(1-2) (1996) 88-90.

[18] P.-T. Chou, S. L. Studer, M. L. Martinez, Practical and Convenient 355-nm and 337-nm Sharp-Cut Filters for Multichannel Raman Spectroscopy, Appl Spectr. 45(3) (1991) 513-515.

[19] F. J. Aparicio, M. Alcairea, A. R. González-Elipe, A. Barranco, M. Holgado, R. Casquel, F. J. Sanz, A. Griol, D. Bernier, F. Dortu, S. Cáceres, M. Antelius, M. Lapis, H. Sohlström, F. Niklaus, Dye-based photonic sensing systems, Sensors and Actuators B 228 (2016) 649–657 and refs. therein.

[20] E. Karakuş, M. Üçüncü, M. Emrullahoğlu, Electrophilic Cyanate As a Recognition Motif for Reactive Sulfur Species: Selective Fluorescence Detection of H_2S, Anal. Chem. 88(1) (2016) 1039-1043 and refs. therein.
[21] F. S. Santos, E. Ramasamy, V. Ramamurthy, F. S. Rodembusch, Excited state chemistry of flavone derivatives in a confined medium: ESIPT emission in aqueous media, Photochem. Photobiol. Sci. 13 (2014) 992-996 and refs. therein.
[22] A. Capan, M. S. Bostan, E. Mozioglu, M. Akgoz, A. C. Goren, M. S. Eroglu, T. Ozturk, Sequence specific recognition of ssDNA by fluorophore 3-hydroxyflavone, J. Photochem. Photobiol. B Biol. 153 (2015) 391–396. Corr. J. Photochem. Photobiol. B: Biol. 158 (2016) 280 and refs. therein.
[23] M. A. Bellucci, D. F. Coker, Molecular dynamics of excited state intramolecular proton transfer: 3-hydroxyflavone in solution, J. Chem. Phys. 136(19) (2012) 194505.
[24] S. Höfener, P. C. Kooijman, J. Groen, F. Ariese, L. Visscher, Fluorescence behavior of (selected) flavonols: a combined experimental and computational study, Phys. Chem. Chem. Phys. 15 (2013) 12572-12581.
[25] R. Salaeh, C. Prommin, W. Chansen, K. Kerdpol, R. Daengngern, N. Kungwan, The effect of protic solvents on the excited state proton transfer of 3-hydroxyflavone: A TD-DFT static and molecular dynamics study, J. Mol. Liq. 252 (2018) 428–438.
[26] A. Warshel, M. Levitt, Theoretical studies of enzymic reactions:Dielectric, electrostatic and steric stabilization of the carbonium ion in the reaction of lysozyme. J. Mol. Biol. 103 (1976) 227−249.
[27] S. Miertus, E. Scrocco, J. Tomasi, Electrostatic interaction of a solute with a continuum. A direct utilizaion of Ab initio molecular potentials for the prevision of solvent effects. Chem. Phys. 55 (1981) 117−129.
[28] J. Tomasi, M. Persico, Molecular Interactions in Solution: An Overview of Methods Based on Continuous Distributions of the Solvent, Chem. Rev. 94 (1994) 2027−2094.
[29] J. Gao, Hybrid Quantum and Molecular Mechanical Simulations:An Alternative Avenue to Solvent Effects in Organic Chemistry. Acc. Chem. Res. 29 (1996) 298−305.
[30] C. Cramer, D. Truhlar, Implicit solvation models: Equilibria, structure, spectra, and dynamics, Chem. Rev. 99 (1999) 2161−2200.
[31] M. Orozco, F. J. Luque, Theoretical Methods for the Description of the Solvent Effect in Biomolecular Systems. Chem. Rev. 100 (2000) 4187−4226.
[32] J. Tomasi, B. Mennucci, R. Cammi, Quantum Mechanical Continuum Solvation Models. Chem. Rev. 105 (2005) 2999−3094.

[33] H. M. Senn, W. Thiel, QM/MM Methods for Biomolecular Systems. Angew. Chem., Int. Ed. 48 (2009) 1198−1229.

[34] S. L. Studer, W. E. Brewer, M. L. Martinez, P.-T. Chou, Time-resolved study of the photooxygenation of 3-hydroxyflavone, J. Am. Chem. Soc. 111 (19), 1989, 7643–7644

[35] J. Pap, J. Kaizer, G. Speier, DPPH-initiated oxygenation of 3-hydroxyflavone to O-benzoylsalicylic acid, React. Kinet. Catal. Lett. 85 (2005) 115-121.

[36] V. N. Agieienko, Y. V. Kolesnik, O. N. Kalugina, Structure, solvation, and dynamics of Mg2+, Ca2+, Sr2+, and Ba2+ complexes with 3-hydroxyflavone and perchlorate anion in acetonitrile medium: A molecular dynamics simulation study, J. Chem. Phys. 140(19) (2014) 194501.

[37] V. N. Agieienko, O. N. Kalugin, Complexation of $Ni(ClO_4)_2$ and $Mg(ClO_4)_2$ with 3-Hydroxyflavone in Acetonitrile Medium: Conductometric, Spectroscopic, and Quantum Chemical Investigation, J. Phys. Chem. B 118(42) (2014) 12251-12262.

[38] A. P. Seitsonen, A. Idrissi, S. Protti, A. Mezzetti, Solvent effects on the vibrational spectrum of 3-hydroxyflavone, J. Mol. Liq. 275 (2019), 723-728.

[39] K. Chevalier, M. M. N. Wolf, A. Funk, M. Andres, M. Gerhards, R. Diller, Transient IR spectroscopy and ab initio calculations on ESIPT in 3-hydroxyflavone solvated in acetonitrile, Phys. Chem. Chem. Phys. 14 **(**2012) 15007-15020.

[40] S. Protti, A. Mezzetti, Solvent effects on the photophysics and photoreactivity of 3-hydroxyflavone: A combined spectroscopic and kinetic study, J. Mol. Liq. 205 (2015) 110-114.

[41] S. Ameer-Beg, S. M. Ormson, R. G. Brown, P. Matousek, M. Towrie, E. T. J. Nibbering, P. Foggi, F. V. R. Neuwahl, J. Phys. Chem. A, 105 (15), (2001) 3709–3718;

[42] V. I. Tomin, D. V. Ushakou, Characterization of ESIPT reactions with instant spectra of fluorescence and complexation processes, J. Luminescence 178 (2016) 94–105 and references therein.

[43] V. I. Tomin, R. Javorsky Temporal characteristics of the fluorescence of the anionic form of 3-hydroxyflavone, Opt. Spectrosc. 103(6) 2007, 952-957.

[44] Z. Szakác, M. Kállay, M. Kubinyi, Theoretical study on the photooxygenation and photorearrangement reactions of 3-hydroxyflavone, RSC Adv. 7 (2017) 32185-32192.

[45] B. Mennucci, E. Cancès, J. Tomasi, Evaluation of Solvent Effects in Isotropic and Anisotropic Dielectrics and in Ionic Solutions with a Unified Integral Equation Method: Theoretical Bases, Computational Implementation, and Numerical Applications. J. Phys. Chem. B 101(49) (1997), 10506−10517.

[46] E. Cancès, B. Mennucci, J. Tomasi, A new integral equation formalism for the polarizable continuum model: Theoretical background and applications to isotropic and anisotropic dielectrics. J. Chem. Phys. 107 (1997) 3032−3041.
[47] C. Lee, W. Yang, R. G. Parr, Development of the Colle-Salvetti correlation-energy formula into a functional of the electron density, Phys. Rev. B 37 (1988), 785
[48] C. Adamo, V. Barone, Toward reliable density functional methods without adjustable parameters: The PBE0 model, J. Chem. Phys. 110 (1999), 6158
[49] Y. Zhao, D. G. Truhlar, The M06 suite of density functionals for main group thermochemistry, thermochemical kinetics, noncovalent interactions, excited states, and transition elements: two new functionals and systematic testing of four M06-class functionals and 12 other functionals, Theor. Chem. Acc. 120(1-3) (2008), 215-241.
[50] T. Yanai, D. P. Tew, N. C. Handy, A new hybrid exchange–correlation functional using the Coulomb-attenuating method (CAM-B3LYP), Chem. Phys. Lett. 393 (2004) 51–57.
[51] J.-D. Chaia, M. Head-Gordon, Systematic optimization of long-range corrected hybrid density functionals, J. Chem. Phys. 128 (2008), 084106.
[52] M. J. Frisch, G. W. Trucks, H. B. Schlegel, G. E. Scuseria, M. A. Robb, J. R. Cheeseman, G. Scalmani, V. Barone, G. A. Petersson,H. Nakatsuji, et al. Gaussian 16, Revision A.03; Gaussian Inc., Wallingford, CT, 2016.
[53] C. A. Guido, D. Jacquemin, C. Adamo, B. Mennucci, Electronic Excitations in Solution: The Interplay between State Specific Approaches and a Time-Dependent Density Functional Theory Description. J. Chem. Theory Comput. (11) 2015, 5782−5790.
[54] M. Caricato, B. Mennucci, J. Tomasi, F. Ingrosso, R. Cammi, S. Corni, G. Scalmani, Formation and relaxation of excited states in solution: a new time dependent polarizable continuum model based on time dependent density functional theory. J. Chem. Phys. 124 (2006) 124520.
[55] R. Improta, V. Barone, G. Scalmani, M. J. Frisch, A state-specific polarizable continuum model time dependent density functional theory method for excited state calculations in solution. J. Chem. Phys. 125 (2006) 054103.
[56] A. V. Marenich, C. J. Cramer, D. G. Truhlar, C. A. Guido, B. Mennucci, G. Scalmani, M. J. Frisch, Practical computation of electronic excitation in solution: vertical excitation model. Chem. Sci. 2 (2011) 2143−2161.
[57] Q. Zeng, W. Liang, Analytic energy gradient of excited electronic state within TDDFT/MMpol framework: Benchmark tests and parallel implementation. J. Chem. Phys. 2015, 143, 134104−134115.

[58] D. Loco, E. Polack, S. Caprasecca, L. Lagardère, F. Lipparini, J.-P. Piquemal,; B. Mennucci, A QM/MM Approach Using the AMOEBA Polarizable Embedding: From Ground State Energies to Electronic Excitations. J. Chem. Theory Comput. 12 (2016), 3654−3661.
[59] B. Lunkenheimer, A. Köhn, Solvent Effects on Electronically Excited States Using the Conductor-Like Screening Model and the Second-Order Correlated Method ADC(2). J. Chem. Theory Comput. 9 (2013) 977−994.
[60] T. Schwabe, General theory for environmental effects on (vertical) electronic excitation energies. J. Chem. Phys. 145 (2016), 154105−154107.
[61] Guareschi, R.; Valsson, O.; Curutchet, C.; Mennucci, B.; Filippi, C. Electrostatic versus Resonance Interactions in Photoreceptor Proteins: The Case of Rhodopsin. J. Phys. Chem. Lett. 7 (2016) 4547−4553**.**
[62] A. Savin, in Recent Developments and Applications of Modern Density Functional Theory, Ed. J. M. Seminario (Elsevier, Amsterdam, 1996), pp. 327-357
[63] C. M. Isborn, B. D. Mar,. B. F. E. Curchod, I. Tavernelli, T. J. Martínez, The Charge Transfer Problem in Density Functional Theory Calculations of Aqueously Solvated Molecules, J. Phys. Chem. B 117 (40) (2013) 12189-12201.
[64] Y. Tawada, T. Tsuneda, S. Yanagisawa, Simultaneous benchmarking of ground- and excited-state properties with long-range-corrected density functional theory, J. Chem. Phys. 129 (2008) 034107.
[65] M. A. Rohrdanz, J. M. Herbert, Simultaneous benchmarking of ground- and excited-state properties with long-range-corrected density functional theory, J. Chem. Phys. 129(3) (2008) 034107.
[66] M. A. Rohrdanz, K.M. Martins, J. M. Herbert, A Long-Range-Corrected Density Functional That Performs Well for Both Ground-State Properties and Time-Dependent Density Functional Theory Excitation Energies, Including Charge-Transfer Excited States, J. Chem. Phys. 130(5), 054112
[67] A. Dreuw, J.L. Weisman, M. Head-Gordon, Long-range charge-transfer excited states in time-dependent density functional theory require non-local exchange J. Chem. Phys. 119, (2003) 2943.
[68] A. Dreuw, M. Head-Gordon, Single-Reference ab Initio Methods for the Calculation of Excited States of Large Molecules, Chem. Rev. 105 (2005) 4009−4037
[69] R. L. Martin, Natural transition orbitals, J. Chem. Phys. 118 (2003), 4775-4777.

[70] C.A. Guido, P. Cortona, C. Adamo. Effective electron displacements: A tool for time-dependent density functional theory computational spectroscopy, J. Chem. Phys. 140 (2014)104101

[71] M. Savarese, C. A. Guido, E. Brémond, I. Ciofini, C. Adamo, Metrics for Molecular Electronic Excitations: A Comparison between Orbital- and Density-Based Descriptors, J. Phys. Chem. A 121(40) 2017, 7543−7549.

[72] S. A. Mewes, F. Plasser, A. Krylov, A. Dreuw, Benchmarking Excited-State Calculations Using Exciton Properties, J. Chem. Theory Comput. 14 (2018) 710−725.

[73] F. Plasser, S.A. Bappler, M. Wormit, A. Dreuw New tools for the systematic analysis and visualization of electronic excitations. II.Applications. J. Chem. Phys. 141 (2014) 024107